NW Pacific-Panthalassa intra-oceanic subduction during Mesozoic times from mantle convection and geoid models

Yi-An Lin[1,*], Lorenzo Colli[1], Jonny Wu[1,*]

[1]University of Houston, TX; [*]Corresponding author

Abstract

Pacific-Panthalassa plate tectonics back to Jurassic times are recognized as the most challenging on Earth to reconstruct, due partly to a large (>9000 km length) unconstrained area between the Pacific and Laurasia (now NE Asia) during the Early Jurassic. We built four contrasted NW Pacific-Panthalassa global plate reconstructions and assimilated their velocity fields into global geodynamic models. We compare our predicted mantle structure, synthetic geoid and dynamic topography to Earth observations. P-wave tomographic filtering of predicted mantle structures allowed for more explicit comparisons to global tomography. Plate reconstructions that include intra-oceanic subduction in NW Pacific-Panthalassa fit better to the observed geoid and residual topography, challenging the Andean-style subduction along East Asia. Our geodynamic models predict significant SE-ward lateral slab advections within the NW Pacific basin lower mantle (~2500 km from Mesozoic times to present), which can confound ‘vertical slab sinking’-style restorations of past subduction zone locations.

1. Introduction

Within Earth's tectonic history during the Mesozoic and Cenozoic eras, the evolution of the Pacific Ocean and its predecessor ocean, Panthalassa, is the most challenging to reconstruct (Müller et al., 2016). The Pacific Ocean currently covers >25% of the present Earth surface and is the largest ocean basin on Earth; but it was even larger during the late Mesozoic, when the Pacific-Panthalassa oceanic realm covered ~45% of Earth (Torsvik et al., 2019). This shrinking of the Pacific-Panthalassa realm since the Mesozoic has been accommodated by subduction. Lost Pacific-Panthalassa oceanic lithosphere is one of the most significant contributors to global plate tectonic uncertainty (Torsvik et al., 2019). This paper discusses the plate tectonic history of NW Pacific-Panthalassa and its implications for subduction histories and accreted oceanic terranes along East Asia (Fig. 1a) using forward geodynamic models to assimilate contrasted NW Pacific-Panthalassa plate reconstructions and explicitly test them against mantle structure, the geoid and dynamic topography.

Seafloor magnetic lineations indicate that the oldest Pacific plate is a triangle-shaped area with ages ~190 Ma (Wright et al., 2016), known as the 'Pacific triangle' (Figs. 1a, b). Pacific-Panthalassa plate reconstructions back to Jurassic times show that only the Pacific triangle has been preserved, with the adjacent oceanic lithosphere (>90% of the total area) now completely subducted and lost (grey areas in Fig. 1b). Within the NW Pacific-Panthalassa, global reconstructions indicate a >9000 km length of unconstrained

area between the Pacific triangle and Laurasia (now NE Asia) during the Early Jurassic (Fig. 1b). The Pacific triangle magnetic lineations imply the Pacific plate grew from the spreading of three connected ridges, whose conjugate rift flanks were named Izanagi, Phoenix, and Farallon. Except for remnants of the Farallon plate, these conjugate plates are completely subducted. Their spatial extent and evolution back in time are thus very uncertain. A simple and straightforward hypothesis is mirroring and interpolating the NW Pacific plate magnetic anomalies to create synthetic seafloor isochrons (e.g. Müller et al., 2016), allowing fully-kinematic, globally-consistent plate histories to be modeled for the Izanagi plate; however, actual details remain poorly known and are briefly reviewed below.

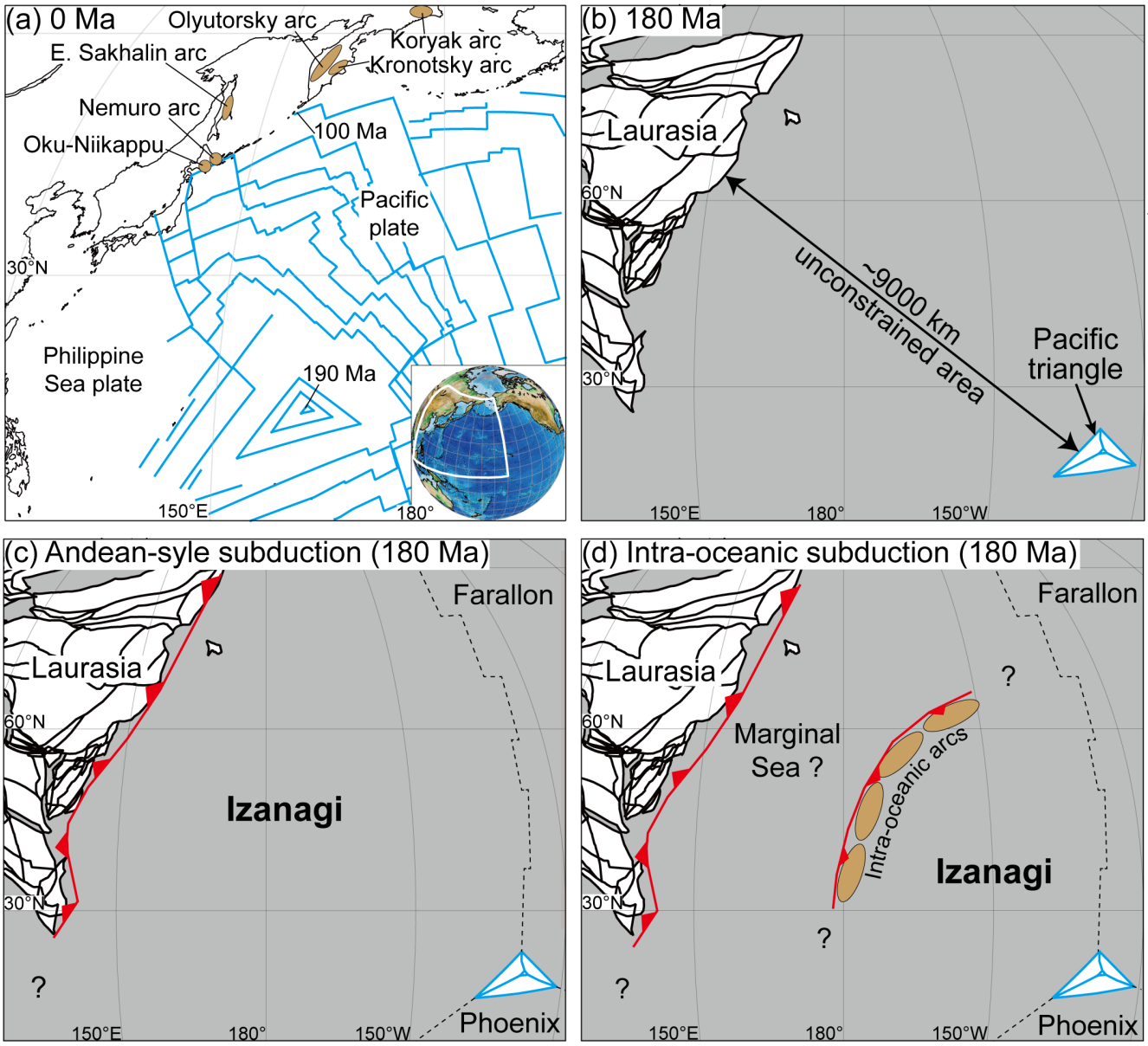

Figure 1. (a) Present-day isochrons (blue lines) of the Pacific plate from Müller et al. (2016) and accreted terranes on the NE Asian continent (in text). (b) Plate reconstruction of western Pacific Ocean during Jurassic time shows ~9000 km unconstrained area between Jurassic Pacific plate and Eurasia. The Pacific triangle is the earliest formed part of the Pacific plate. (c) Reconstructed Andean-style subduction along Laurasia during the Jurassic (Müller et al., 2016), in contrast to (d) intra-oceanic subduction within Pacific-Panthalassa (e.g. van der Meer et al., 2012).

1.1 Plate tectonic reconstructions of the NW Pacific Ocean basin

‘Andean-style’ plate tectonic reconstructions indicate the size and motion of the Pacific and Izanagi plates by attributing all Pacific-Panthalassa-Eurasian convergence (>9000 km since the Jurassic) to subduction along the Eurasian margin; no intra-oceanic subduction occurred within NW Pacific-Panthalassa (Fig. 1c). These assumptions imply a large, long-lived Izanagi plate extending from central Panthalassa to the Eurasian margin and converging continually towards Eurasia (Fig. 1c) (e.g. Engebretson et al., 1984; Müller et al., 2016; Seton et al., 2012; Whittaker et al., 2007). To date, almost all published geodynamic models implement Andean-style plate reconstructions for the NW Pacific (e.g. Flament, 2018; Lin et al., 2020; Matthews et al., 2016).

In contrast, a second class of ‘intra-oceanic subduction’ plate reconstructions imply intra-oceanic arcs within Pacific-Panthalassa (Fig. 1d). These plate reconstructions are based on accreted Mesozoic-aged intra-oceanic arcs along East Asia (brown polygons in Fig. 1a) and supported by fast, slab-like anomalies in mantle tomographic images under the present Pacific or near the East Asian margin (e.g. Domeier et al., 2017; Ueda & Miyashita, 2005; van der Meer et al., 2012; Yamasaki & Nanayama, 2018). Island arcs apparently accreted along easternmost Eurasia during the earliest Cretaceous ~145 Ma at NE Japan (Ueda & Miyashita, 2005), along the Russian Far East during the mid-Cretaceous (Filatova & Vishnevskaya, 1997); and along Hokkaido, Kamchatka, and East Sakhalin during the Late Cretaceous to the mid-Eocene (Alexeiev et al., 2006; Konstantinovskaia, 2000; Nokleberg, 2010; Shapiro & Solov’ev, 2009; Zharov, 2005).

Some plate reconstructions that explain these accreted island arcs imply the existence of NW Pacific-Panthalassa intra-oceanic subduction zones and additional plates other than Izanagi (Fig. 1d) (e.g. Domeier et al., 2017; Vaes et al., 2019; van der Meer et al., 2012). However, other studies explain the Japan accretionary complexes by a >1000 km northwards translation from South China or Tethys by sinistral strike-slip along the eastern Eurasian margin within an Andean-style NW Pacific plate tectonic context (e.g. Fujisaki et al., 2014; Sakashima et al., 2003). Only limited attempts (e.g. Seton et al., 2018) have been made to test the viability of intra-oceanic subduction within the NW Pacific using global geodynamic models due, in part, to the challenges of building plate reconstructions with limited constraints (e.g. Fig. 1b). In this study, we approach this challenge by creating a series of increasingly complex plate reconstructions featuring intra-oceanic subduction in the NW Pacific-Panthalassa. We then assimilate them into global geodynamic models and probe for improved fits to imaged mantle structure and Earth's geoid. We discuss implications for plate tectonics, the history of mantle flow, and NE Asian dynamic topography.

2. Method

Mantle circulation models use global plate velocities as input in the form of time-dependent boundary conditions to link surface processes and the deep Earth (e.g. Bunge & Grand, 2000; Nerlich et al., 2016; Zahirovic et al., 2016). Previous geodynamic studies that addressed NW Pacific plate tectonics typically rely on assimilation of a single input plate tectonic reconstruction while testing other parameter spaces (e.g.

viscosity) (Cao et al., 2018; Seton et al., 2015). Here we take a different approach from previous studies and assimilate four contrasted global plate reconstructions within three whole-mantle viscosity profiles (Cases a to c. See Fig. S2; Table S1), for a total of twelve geodynamic models. Three of the four global plate reconstructions are built specifically for this study (see Supplemental for details). Our fourth plate reconstruction was previously published (Matthews et al., 2016) and is our reference model.

We test two end-member classes of plate reconstructions that we call 'Andean-style' and 'intra-oceanic' subduction (Figs. 2, S1). *Andean-style subduction* of the Izanagi (IZA) plate along the Eurasian continental margin is assimilated from a global reconstruction from 460 to 0 Ma based on Matthews et al. (2016) (Figs. S1a-e), which is called 'Reconstruction 1'. In this model, all western Pacific-Eurasia plate convergence after the Jurassic is consumed by a single subduction zone along the eastern Eurasian margin (Movie 1). This reconstruction results in the largest IZA plate relative to the other reconstructions (Fig. 2a). *Intra-oceanic subduction* within the western Pacific Ocean is featured by 'Reconstructions 2, 3 and 4' (Fig. 2). Various intra-oceanic subduction-style plate reconstructions for the western Pacific Ocean have been proposed due to sparse geological and kinematic constraints (e.g. Fig. 1). As such, we built a suite of three plate reconstructions with increasing complexity based on published regional plate reconstructions (Movies 2 to 4). They all follow the Andean-style Reconstruction 1 from 460 Ma until Jurassic times (at 160, 180, or 190 Ma; Table S2) and then implement alternative plate kinematic histories during mid-Mesozoic to early Cenozoic times (see Supplemental for details).

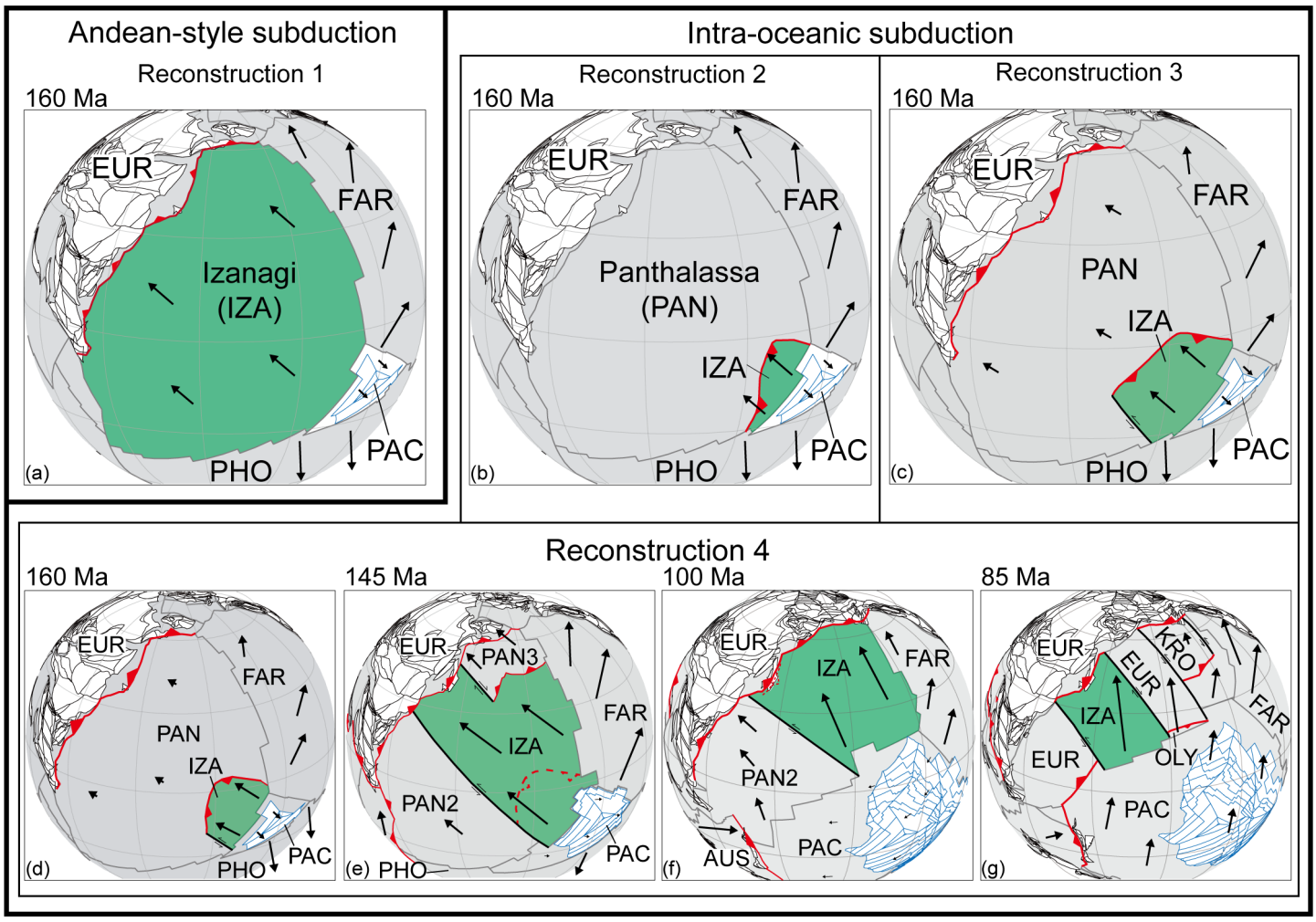

Figure 2. Representative maps showing the four main plate reconstructions assimilated into the geodynamic models in this study. (a) Andean-style subduction (Reconstruction 1) is the default model from Matthews et al. (2016). (b)-(g) Reconstructions 2 to 4 implemented intra-oceanic subduction in western Pacific Ocean. (b) Reconstruction 2 implemented a size-limited Izanagi plate (IZA) overriding Panthalassa plate (PAN), which is stationary relative to Eurasia (EUR). (c) Reconstruction 3 implemented intra-oceanic subduction of IZA during 180-145 Ma while keeping the Eurasian margin active (although at a reduced convergence rate with respect to Reconstruction 1), followed by Andean style subduction after 145 Ma. (d)-(g) Reconstruction 4 builds upon Reconstruction 3 and accounts for the terrane accretion at Kamchatka, magmatic records along Eurasia and recently published NE Asia plate reconstructions (e.g. Vaes et al., 2019). PAC: Pacific plate; FAR: Farallon plate; PHO: Phoenix plate; IND: Indian plate; AUS: Australia plate; PAN: Panthalassa plate; KUL: Kula plate; KRO: Kronotsky plate; OLY: Olyutorsky plate; PAN2: Panthalassa plate 2; PAN3: Panthalassa plate 3.

3. Results

3.1 Predicted and imaged mantle structure

A cross-section A-A' across East Asia and the NW Pacific shows the present-day mantle thermal structure and flow fields (Fig. 3 left column) predicted by geodynamic Models 1a to 4a (i.e. Reconstructions 1 to 4 within geodynamic Case a, our preferred viscosity profile; alternative viscosity profile Cases b and c are shown in Supplemental). Despite significant variations in assimilated plate reconstructions (Fig. 2), all models display relatively similar first-order mantle structures and flows (Fig. 3 left column) that are characterized by: (1) shallower, stagnant Pacific slabs under the Eurasian margin around 500 km depths; (2) large swaths of slab anomalies under or offshore from the Eurasian margin entrained by downwelling flows; and, (3) slabs within the lowermost lower mantle (>2000 km depths) under the central Pacific entrained in SE-directed flows towards a plume within the central Pacific. In all models, the time-dependent mantle evolution since the Late Jurassic shows SE-directed lower mantle 'return flows' towards a plume in the central Pacific (Figs. S6, S7). These flows help to explain the relatively similar mantle structures in Models 1a to 4a (Fig. 3) because the lower mantle return flows advect all subducted slabs laterally towards the southeast (Figs. S6, S7). The most extreme case is the Andean-style Model 1a, where Pacific-Panthalassa subduction is continuously pinned to the Eurasian margin but the subducted slabs are advected laterally within the lower mantle into the central Pacific by >2000 km since Jurassic (Figs. 3, S6).

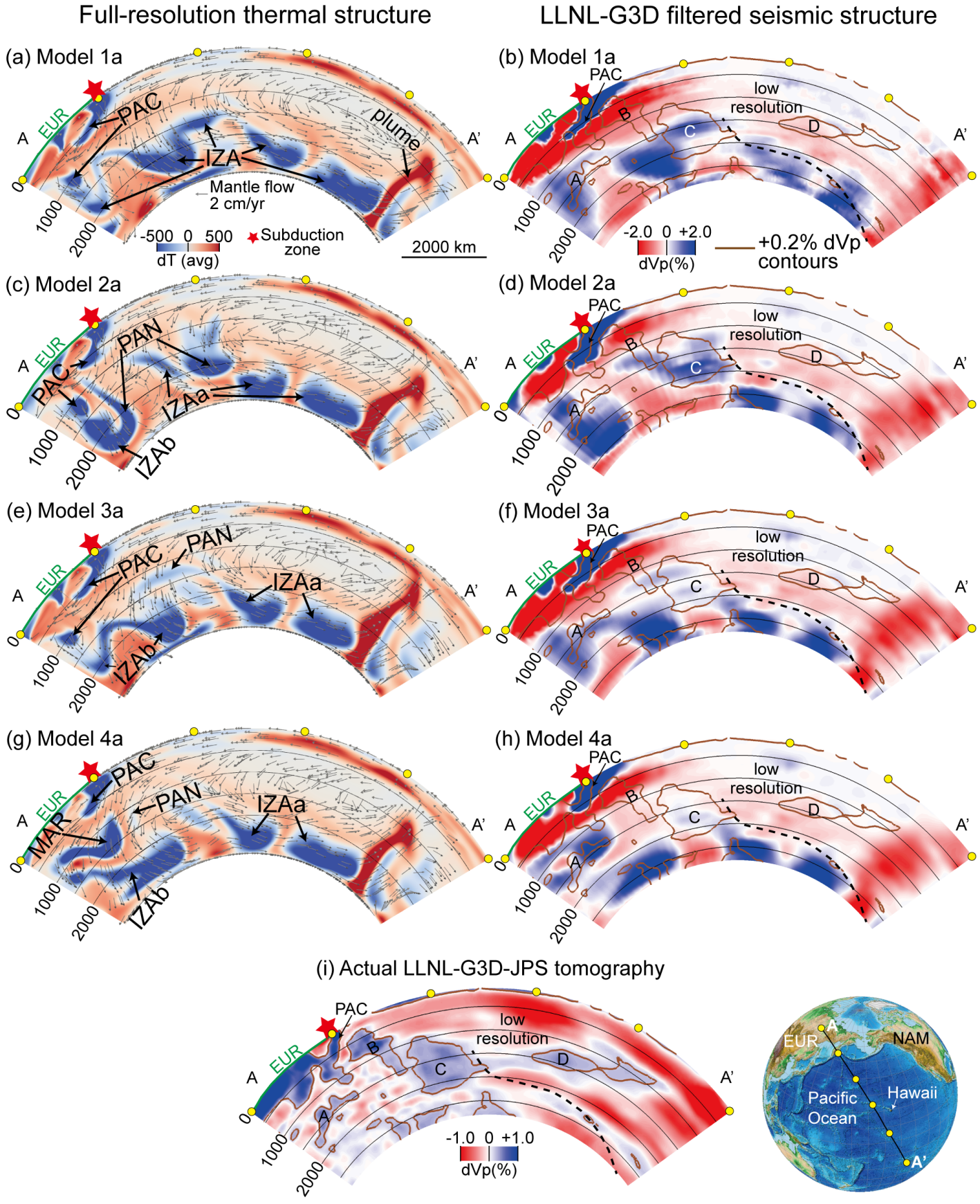
Full-resolution thermal structure
LLNL-G3D filtered seismic structure
(a) Model 1a
(b) Model 1a
(c) Model 2a
(d) Model 2a
(e) Model 3a
(f) Model 3a
(g) Model 4a
(h) Model 4a
(i) Actual LLNL-G3D-JPS tomography
PAC
PAN
MAR
EUR
NAM
IZA
IZAa
IZAb
plume
Mantle flow
2 cm/yr
-500 0 500
dT (avg)
Subduction zone
2000 km
low resolution
A
A'
B
C
D
-2.0 0 +2.0
dVp(%)
+0.2% dVp contours
-1.0 0 +1.0
0
1000
2000
Pacific Ocean
Hawaii

Figure 3. Cross sections of the geodynamically modeled present-day mantle structure for Model 1a to 4a. The left column shows the full-resolution thermal structure while the right column shows the tomographically-filtered seismic structure. (a) Model 1a produces extensive IZA slabs in the lower mantle beneath Eurasia and NW Pacific and PAC slabs at upper 1000 km depths beneath Eurasian margin; (c) Model 2a produces PAN slabs at 1000-2000 km depths, IZAa to the east of PAN slabs and IZAb to the west of PAN slabs in the lower mantle; (e) Model 3a and (g) Model 4a produce IZAa in the lower mantle to the east of IZAb, and (g) Model 4a produces MAR slabs at ~700-1600 km depths beneath Eurasia. LLNL-G3D filtered dVp for (b) Model 1a, (d) Model 2a, (f) Model 3a, and (h) Model 4a are compared to (i) LLNL-G3D-JPS (Simmons et al., 2015) seismic tomography. Izanagi slabs-a (IZAa) and Izanagi slabs-b (IZAb) are used to differentiate the Izanagi subduction before and after 160 Ma. MAR: Marginal sea slabs formed by closing NE Eurasian backarc basin. Brown lines in (b), (d), (f) and (h) show +0.2% dVp contours from (i).

The right column of Figure 3 shows 'synthetic tomography' images of Models 1a to 4a produced by converting the left-column temperature anomalies to seismic anomalies using a thermodynamically self-consistent model of mantle mineralogy (Chust et al., 2017; Stixrude & Lithgow-Bertelloni, 2011) and subsequently filtered with the LLNL-G3D-JPS resolution operator (Simmons et al., 2019). After tomographic-filtering, the shallow Pacific (PAC) slabs are still relatively well-imaged whereas the lower mantle slabs (Fig. 3 right column) show more blurring relative to the full-resolution models. LLNL-G3D-JPS seismic tomography (Simmons et al., 2015) shows the shallow PAC slabs and four swaths of lower mantle fast anomalies A to D (Fig. 3i). We exclude fast anomaly D from comparison due their occurrence within a recognized low resolution region in the central Pacific (van der Meer et al., 2012). However, after tomographic filtering, it is difficult to visually distinguish which predicted mantle state best fits actual tomography (Fig. 3). Comparisons of tomographically-filtered horizontal slices at various lower mantle depths within the NW Pacific basin show similar conclusions (Fig. S15). Computed correlations for Models 1a to 4a and LLNL-G3D-JPS seismic tomography of

208 ~0.04-0.05 confirm that no single model shows a superior fit to tomography. Thus, we
209 conclude from the tomographic blurring produced by our tomographic filtering (e.g. Figs.
210 3, S15) that predicted and imaged mantle structure comparisons within the central
211 Pacific are likely hindered by limited tomographic resolution.
212
213 *3.2 Comparison between synthetic and observed geoid*
214
215 For each modeled present-day mantle structure we followed Thoraval and Richards
216 (1997) and computed the synthetic geoid and its correlation to the observed geoid (Fig.
217 4). The geoid response is sensitive to density and viscosity structure. As the forward
218 geoid problem is less computationally demanding, for each plate reconstruction we
219 computed 42 synthetic geoid responses employing a total of 14 viscosity profiles,
220 exploring a range of more extreme viscous layering scenarios (Fig. S3) for
221 geodynamically-derived mantle structures in 3 Cases (Fig. 4). Correlations range from
222 0.47 (viscosity profile 6 in Case a) to slightly negative, with an average correlation of
223 around 0.25 (Fig. 4), which is on par with a previous study (e.g. Flament, 2018). Despite
224 correlation variability between synthetic geoid, the Andean-style Reconstruction 1
225 produces the least satisfactory correlation in all cases (compare blue and reddish color
226 in Fig. 4). Within the better fitting intra-oceanic Reconstructions 2 to 4, Reconstruction 4
227 shows the best correlation in the majority of cases (23/42 in Fig. 4) whereas
228 Reconstruction 2 is superior in about one-third (13/42 in Fig. 4). Therefore, we choose
229 Reconstruction 4 as our preferred intra-oceanic reconstruction for the next section,
230 while acknowledging that no intra-oceanic reconstruction discussed here is universally-

231 superior. Regardless, our analysis indicates that as a plate reconstruction class, the
232 intra-oceanic Reconstructions 2 to 4 are distinctively superior to the Andean-style
233 Reconstruction 1 on the basis of predicted and observed geoid.
234

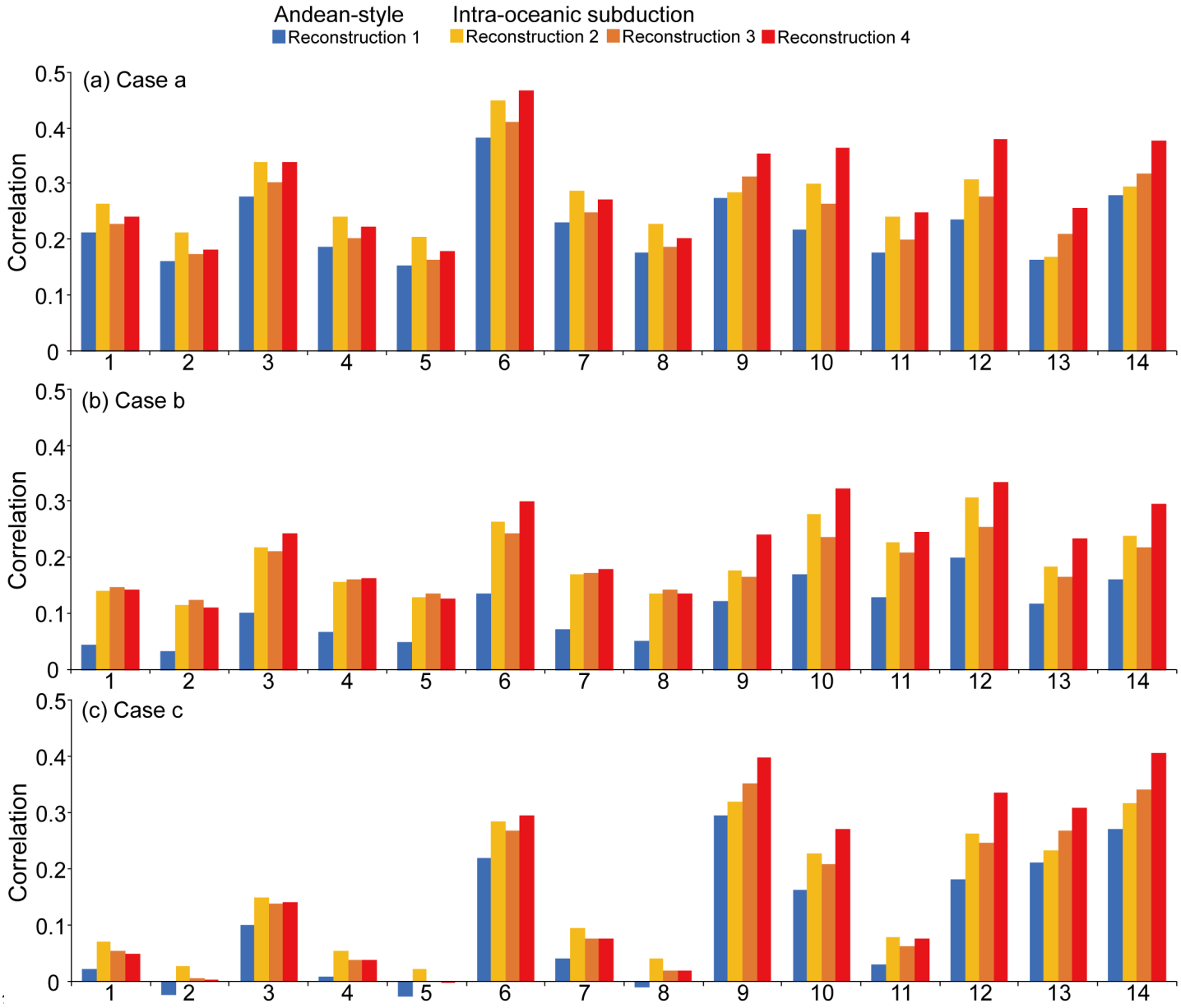

236 Figure 4. Correlation between observed non-hydrostatic geoid and synthetic geoid from
237 the present-day structures predicted by Reconstructions 1 to 4 for (a) Case a, (b) Case
238 b and (c) Case c with various radial viscosity profiles 1 to 14. In all combinations, intra-
239 oceanic Reconstructions 2 to 4 achieved higher correlations to the observed geoid
240 relative to the Andean-style Reconstruction 1.

241

242 *3.3 Comparison of modeled dynamic topography and observed residual topography*

243

244 We focus here on the present-day dynamic topography predicted by our best-fit model
245 (viscosity profile 6 in Case a) and compare the results of the Andean-style Model 1a
246 and intra-oceanic Model 4a end-members (Fig. 5) against observed residual topography
247 (e.g. Hoggard et al., 2016). Global correlation between our predicted dynamic
248 topography and observed residual topography model (Hoggard et al., 2016) for degree
249 1-3 and is 0.49-0.56, which is comparable to a previous study (0.31-0.55) (Flament,
250 2018) indicating a reasonable result. Focusing on dynamic topography predictions in the
251 western Pacific, we show the present-day dynamic topography up to degree 160 and
252 compare it to 83 most accurate spot measurements of Hoggard et al. (2017) (Fig. 5).
253 The root-mean-square deviation (RMSD) between dynamic and residual topography is
254 1054 m for Model 1a and 676 m for Model 4a (Fig. 5), indicating that intra-oceanic
255 Model 4a produces a superior fit. In particular, the Andean-style Model 1a misfits can be
256 primarily traced to excess dynamic topography within the Pacific Ocean offshore Japan,
257 with less prominent misfit contributions within the central Philippine Sea plate and
258 Bering Sea. Comparison of all Models 1a to 4a show that the intra-oceanic Models 2a to
259 4a uniformly produce a 20-25% improved fit between dynamic and residual topography
260 within the western Pacific Ocean (Fig. S16).

261

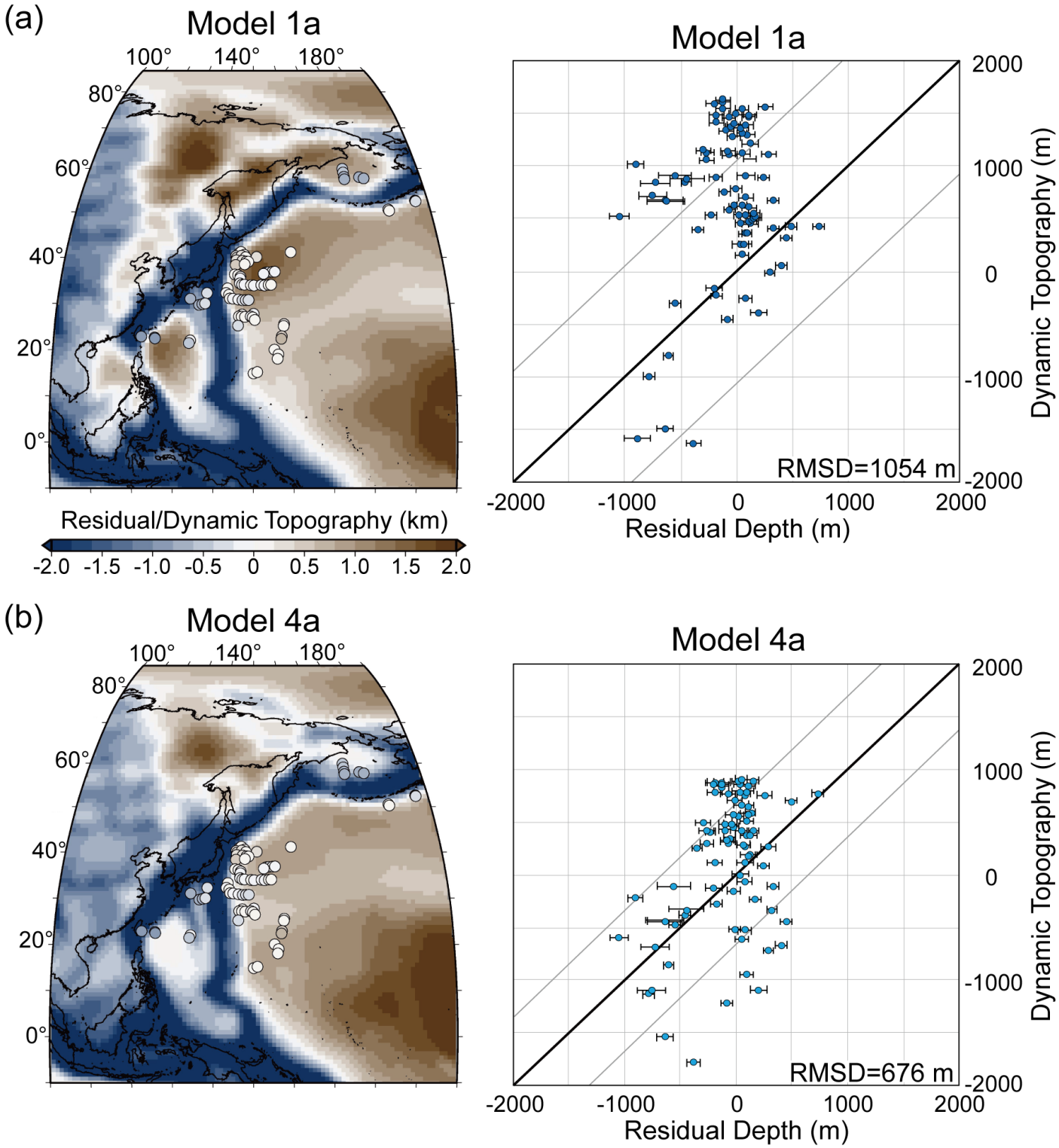

Figure 5. (a) and (b) show maps of the dynamic topography in western Pacific predicted from Model 1a and Model 4a using viscosity profile 6. Colored circles show 83 spot residual topography measurements from Hoggard et al. (2017). (c) and (d) show scatter plots between dynamic topography and the 83 spot residual topography measurements in a), b). Black line delineates a 1:1 correlation; grey lines bound 1 root-mean-square

deviation (RMSD). Intra-oceanic Model 4a shows a superior match to residual topography (i.e. lower RMSD error) compared to Andean-style Model 1a.

4. Discussion

4.1 Implications for intra-oceanic subduction within the NW Pacific Ocean basin

Our geoid and dynamic topography comparisons robustly show that intra-oceanic Reconstructions 2 to 4 produce better matches to the real Earth than the Andean-style Reconstruction 1 (Figs. 4, 5). Within the intra-oceanic Reconstructions, our results seem to show that our most complex reconstruction (Reconstruction 4) generally produces the best fit to the geoid, but more work is necessary to discern specific plate reconstruction details between Reconstructions 2 to 4. Our results suggest that at least some accreted oceanic terranes along the NW Pacific margin (Fig. 1a) could have originated from Pacific-Panthalassan or East Asian backarc intra-oceanic subduction zones, providing alternative explanations for East Asian margin allochthonous terranes (e.g. Sakashima et al., 2003). This affirms previous tomography-based plate reconstructions from better-imaged areas of the NW Pacific Ocean that showed probable Pacific-Panthalassa intra-oceanic subduction during Mesozoic times (van der Meer et al., 2012), which have implications for global CO_2 level estimates since the Triassic (Van Der Meer et al., 2014). Regardless, our conclusions present important challenges to the Andean-style margin assumptions that are deeply embedded into almost all current East Asian plate tectonic, geodynamic and geological studies (Cao et al., 2018; Müller et al., 2019; Wu et al., 2019).

Despite successful tests of predicted and imaged mantle structure within other East Asian regions (e.g. Lin et al., 2020; Seton et al., 2015), our test under the NW Pacific Ocean (Fig. 3) was inconclusive. Considering the extreme contrasts in assimilated plate reconstructions (Fig. 2), the inability to differentiate between end-member plate reconstructions from mantle structure is noteworthy, and is partly due to the limited resolution of tomographic images in the lower mantle. Future improvements in central Pacific seismic tomography may help constrain alternative reconstructions. However, one important complicating factor is the lateral advection of lower mantle slabs within the central Pacific Ocean, which contributes to the similarity of modeled present-day mantle states (Fig. 3). The lateral advection was produced in all four reconstructions (Fig. 3) and challenges 'vertical slab sinking' simplifying assumptions that have been used in some tomography-based slab-plate reconstructions of Pacific-Panthalassa (e.g. Sigloch & Mihalynuk, 2013; van der Meer et al., 2012). Significant lateral advection of slab material is present in previous models (Seton et al., 2015; Zahirovic et al., 2016) and slabs are advected SE-wards in all our models by around 2500 km in the lower mantle (Figs. 3, S6-11). The amount of lateral advection of slab material depends on choices of geodynamic modelling parameters. Steinberger et al. (2012) reports lateral advection of only a few degrees, on average, whereas Wang et al. (2018) illustrate how mantle upwellings can act as attractors of subducted slab material, even in the presence of thermo-chemical piles. Therefore, caution is needed when tomographic images are used for restoring the absolute positions of ancient subduction zones, as

different interpretative assumptions can imply different styles of convection in the Earth's mantle.

Our comparison between predicted and imaged mantle structure within the central Pacific Ocean, which was made more explicit than previous attempts by our P-wave tomographic filtering (Fig. 3 right column), illustrates how tomography-led plate reconstructions of some ocean basins will have limitations due to poorer resolution (Fig. 3). Such tomographic blind spots have also confounded past studies (e.g. van der Meer et al., 2012). Here we show the advantage of employing an array of comparisons to forward geodynamic models (i.e. the geoid and dynamic topography) when faced with potentially ambiguous comparisons to mantle structure. This approach may be important for studies of other large ocean basins, such as the Indian Ocean-Tethys (e.g. Nerlich et al., 2016), where seismic source-receiver pairings may also not be optimal for imaging mantle structure within ocean basin center.

Acknowledgements

We thank Jeremy Tsung-Jui Wu, Yiduo Liu, Spencer Fuston, Hayato Ueda, Gaku Kimura, Ying Song, Kazu Okamoto, Maria Seton and Kasra Hosseini for valuable discussion and support, Nathan Simmons and Thomas Chust for assistance and helpful discussions on mineral physics and tomographic filtering, and the University of Houston (UH) Center for Tectonics and Tomography for organizing scientific workshops. Yi-An Lin and Jonny Wu are supported by U.S. National Science Foundation grant EAR-

1848327. Yi-An Lin, Jonny Wu, and Lorenzo Colli acknowledge funding from the State of Texas Governor's University Research Initiative (GURI), the use of the UH Sabine Clusters, the advanced support from the UH Research Computing Data Core and Gocad software educational licenses from Emerson Paradigm. GPlates files and movies of all plate reconstructions are provided in the Supplemental materials. The vtk file for the modeled present-day mantle temperature and velocity field can be found at Texas Data Repository (https://doi.org/10.18738/T8/KEFMWZ).

References

Akinin, V. V., & Miller, E. L. (2011). Evolution of calc-alkaline magmas of the Okhotsk-Chukotka volcanic belt. *Petrology, 19*(3), 237-277. doi:https://doi.org/10.1134/S0869591111020020

Alexeiev, D. V., Gaedicke, C., Tsukanov, N. V., & Freitag, R. (2006). Collision of the Kronotskiy arc at the NE Eurasia margin and structural evolution of the Kamchatka–Aleutian junction. *International Journal of Earth Sciences, 95*(6), 977-993. doi:https://doi.org/10.1007/s00531-006-0080-z

Boschman, L. M., & van Hinsbergen, D. J. J. (2016). On the enigmatic birth of the Pacific Plate within the Panthalassa Ocean. *Science Advances, 2*(7), e1600022. doi:https://doi.org/10.1126/sciadv.1600022

Boyden, J. A., Müller, R. D., Gurnis, M., Torsvik, T. H., Clark, J. A., Turner, M., . . . Cannon, J. S. (2011). Next-generation plate-tectonic reconstructions using GPlates. In Baru, C. & Keller, G. R. (Eds.), *Geoinformatics: Cyberinfrastructure for the Solid Earth Sciences* (pp. 95-114). Cambridge: Cambridge University Press.

Bunge, H.-P., & Grand, S. P. (2000). Mesozoic plate-motion history below the northeast Pacific Ocean from seismic images of the subducted Farallon slab. *Nature, 405*, 337-340. doi:https://doi.org/10.1038/35012586

Bunge, H.-P., Richards, M. A., Lithgow-Bertelloni, C., Baumgardner, J. R., Grand, S. P., & Romanowicz, B. A. (1998). Time Scales and Heterogeneous Structure in Geodynamic Earth Models. *Science, 280*(5360), 91-95. doi:https://doi.org/10.1126/science.280.5360.91

Cai, G., Wan, Z., Yao, Y., Zhong, L., Zheng, H., Kapsiotis, A., & Zhang, C. (2019). Mesozoic Northward Subduction Along the SE Asian Continental Margin Inferred from Magmatic Records in the South China Sea. *Minerals, 9*(10). doi:https://doi.org/10.3390/min9100598

Cao, X., Flament, N., Müller, D., & Li, S. (2018). The Dynamic Topography of Eastern China Since the Latest Jurassic Period. *Tectonics, 37*(5), 1274-1291. doi:https://doi.org/10.1029/2017TC004830

Chust, T. C., Steinle-Neumann, G., Dolejš, D., Schuberth, B. S. A., & Bunge, H. P. (2017). MMA-EoS: A Computational Framework for Mineralogical Thermodynamics. *Journal of Geophysical Research: Solid Earth, 122*(12), 9881-9920. doi:https://doi.org/10.1002/2017JB014501

Domeier, M., Shephard, G. E., Jakob, J., Gaina, C., Doubrovine, P. V., & Torsvik, T. H. (2017). Intraoceanic subduction spanned the Pacific in the Late Cretaceous–Paleocene. *Science Advances, 3*(11), eaao2303. doi:https://doi.org/10.1038/ngeo111110.1126/sciadv.aao2303

Dong, S., Zhang, Y., Li, H., Shi, W., Xue, H., Li, J., . . . Wang, Y. (2018). The Yanshan orogeny and late Mesozoic multi-plate convergence in East Asia—Commemorating 90th years of the “Yanshan Orogeny”. *Science China Earth Sciences, 61*, 1888-1909. doi:https://doi.org/10.1038/ngeo111110.1007/s11430-017-9297-y

Engebretson, D. C., Cox, A., & Gordon, R. G. (1984). Relative motions between oceanic plates of the Pacific Basin. *Journal of Geophysical Research: Solid Earth, 89*(B12), 10291-10310. doi:https://doi.org/10.1038/ngeo111110.1130/SPE206-p1

Filatova, N. I., & Vishnevskaya, V. S. (1997). Radiolarian stratigraphy and origin of the Mesozoic terranes of the continental framework of the northwestern Pacific (Russia). *Tectonophysics, 269*(1), 131-150. doi:https://doi.org/10.1016/S0040-1951(96)00156-4

Flament, N. (2018). Present-day dynamic topography and lower-mantle structure from palaeogeographically constrained mantle flow models. *Geophysical Journal International, 216*(3), 2158-2182. doi:https://doi.org/10.1038/ngeo111110.1093/gji/ggy526

Fujisaki, W., Isozaki, Y., Maki, K., Sakata, S., Hirata, T., & Maruyama, S. (2014). Age spectra of detrital zircon of the Jurassic clastic rocks of the Mino-Tanba AC belt in SW Japan: Constraints to the provenance of the mid-Mesozoic trench in East Asia. *Journal of Asian Earth Sciences, 88*, 62-73. doi:https://doi.org/10.1016/j.jseaes.2014.02.006

Gurnis, M., Turner, M., Zahirovic, S., DiCaprio, L., Spasojevic, S., Müller, R. D., . . . Bower, D. J. (2012). Plate tectonic reconstructions with continuously closing plates. *Computers & Geosciences, 38*(1), 35-42. doi:10.1016/j.cageo.2011.04.014

Hager, B. H., Richards, M. A., apos, Nions, R. K., Clayton, R., & Parsons, B. (1989). Long-wavelength variations in Earth's geoid: physical models and dynamical implications. *Philosophical Transactions of the Royal Society of London. Series A, Mathematical and Physical Sciences, 328*(1599), 309-327. doi:10.1098/rsta.1989.0038

Hoggard, M. J., White, N., & Al-Attar, D. (2016). Global dynamic topography observations reveal limited influence of large-scale mantle flow. *Nature Geoscience, 9*, 456–463. doi:https://doi.org/10.1038/ngeo2709

Hoggard, M. J., Winterbourne, J., Czarnota, K., & White, N. (2017). Oceanic residual depth measurements, the plate cooling model, and global dynamic topography. *Journal of Geophysical Research: Solid Earth, 122*(3), 2328-2372. doi:https://doi.org/10.1002/2016JB013457

Hosseini, K., Sigloch, K., Tsekhmistrenko, M., Zaheri, A., Nissen-Meyer, T., & Igel, H. (2020). Global mantle structure from multifrequency tomography using P, PP and P-diffracted waves. *Geophysical Journal International, 220*(1), 96-141. doi:10.1093/gji/ggz394

Hourigan, J. K., & Akinin, V. V. (2004). Tectonic and chronostratigraphic implications of new 40Ar/39Ar geochronology and geochemistry of the Arman and Maltan-Ola volcanic fields, Okhotsk-Chukotka volcanic belt, northeastern Russia. *GSA Bulletin, 116*(5-6), 637-654. doi:10.1130/B25340.1

Jarvis, G. T., & McKenzie, D. P. (1980). Convection in a compressible fluid with infinite Prandtl number. *Journal of Fluid Mechanics, 96*(3), 515-583. doi:https://doi.org/10.1017/S002211208000225X

Keating, B. H., Mattey, D. P., Helsley, C. E., Naughton, J. J., Epp, D., Lazarewicz, A., & Schwank, D. (1984). Evidence for a hot spot origin of the Caroline Islands. *Journal of Geophysical Research: Solid Earth, 89*(B12), 9937-9948. doi:https://doi.org/10.1029/JB089iB12p09937

Konstantinovskaia, E. A. (2000). Geodynamics of an Early Eocene arc–continent collision reconstructed from the Kamchatka Orogenic Belt, NE Russia. *Tectonophysics, 325*(1), 87-105. doi:https://doi.org/10.1016/S0040-1951(00)00132-3

Li, C., van der Hilst, R. D., Engdahl, E. R., & Burdick, S. (2008). A new global model forPwave speed variations in Earth's mantle. *Geochemistry, Geophysics, Geosystems, 9*(5), Q0501. doi:https://doi.org/10.1029/2007gc001806

Lin, Y.-A., Colli, L., Wu, J., & Schuberth, B. S. A. (2020). Where Are the Proto-South China Sea Slabs? SE Asian Plate Tectonics and Mantle Flow History From Global Mantle Convection Modeling. *Journal of Geophysical Research: Solid Earth, 125*(12), e2020JB019758. doi:https://doi.org/10.1029/2020JB019758

Matthews, K. J., Maloney, K. T., Zahirovic, S., Williams, S. E., Seton, M., & Müller, R. D. (2016). Global plate boundary evolution and kinematics since the late Paleozoic. *Global and Planetary Change, 146*, 226-250. doi:https://doi.org/10.1016/j.gloplacha.2016.10.002

Müller, R. D., Seton, M., Zahirovic, S., Williams, S. E., Matthews, K. J., Wright, N. M., . . . Cannon, J. (2016). Ocean Basin Evolution and Global-Scale Plate Reorganization Events Since Pangea Breakup. *Annual Review of Earth and Planetary Sciences, 44*(1), 107-138. doi:https://doi.org/10.1146/annurev-earth-060115-012211

Müller, R. D., Zahirovic, S., Williams, S. E., Cannon, J., Seton, M., Bower, D. J., . . . Gurnis, M. (2019). A global plate model including lithospheric deformation along major rifts and orogens since the Triassic. *Tectonics, 38*, 1884–1907. doi:https://doi.org/10.1029/2018TC005462

Nerlich, R., Colli, L., Ghelichkhan, S., Schuberth, B., & Bunge, H.-P. (2016). Constraining central Neo-Tethys Ocean reconstructions with mantle convection models. *Geophysical Research Letters, 43*(18), 9595-9603. doi:https://doi.org/10.1002/2016GL070524

Nokleberg, W. J., (Eds). (2010). *Metallogenesis and Tectonics of Northeast Asia: U.S Geological Survey Professional Paper 1765, 624p*. Reston, Virginia: U.S Geological Survey.

Obayashi, M., Yoshimitsu, J., Nolet, G., Fukao, Y., Shiobara, H., Sugioka, H., . . . Gao, Y. (2013). Finite frequency whole mantlePwave tomography: Improvement of subducted slab images. *Geophysical Research Letters, 40*(21), 5652-5657. doi:https://doi.org/10.1002/2013gl057401

Pail, R., Bruinsma, S., Migliaccio, F., Förste, C., Goiginger, H., Schuh, W.-D., . . . Tscherning, C. C. (2011). First GOCE gravity field models derived by three different approaches. *Journal of Geodesy, 85*(11), 819. doi:10.1007/s00190-011-0467-x

Pekeris, C. L. (1935). Thermal Convection in the Interior of the Earth. *Geophysical Supplements to the Monthly Notices of the Royal Astronomical Society, 3*(8), 343-367. doi:10.1111/j.1365-246X.1935.tb01742.x

Ritsema, J., Deuss, A., van Heijst, H. J., & Woodhouse, J. H. (2011). S40RTS: a degree-40 shear-velocity model for the mantle from new Rayleigh wave dispersion, teleseismic traveltime and normal-mode splitting function measurements. *Geophysical Journal International, 184*(3), 1223-1236. doi:https://doi.org/10.1111/j.1365-246X.2010.04884.x

Sakashima, T., Terada, K., Takeshita, T., & Sano, Y. (2003). Large-scale displacement along the Median Tectonic Line, Japan: evidence from SHRIMP zircon U–Pb dating of granites and gneisses from the South Kitakami and paleo-Ryoke belts. *Journal of Asian Earth Sciences, 21*(9), 1019-1039. doi:https://doi.org/10.1016/S1367-9120(02)00108-6

Schuberth, B. S. A., Bunge, H. P., & Ritsema, J. (2009). Tomographic filtering of high-resolution mantle circulation models: Can seismic heterogeneity be explained by temperature alone? *Geochemistry, Geophysics, Geosystems, 10*(5), Q05W03. doi:https://doi.org/10.1029/2009GC002401

Seton, M., Flament, N., & Whittaker, J. (2018). *Geodynamic history of subducted slabs along the East Asian margin since the Cretaceous*. Paper presented at the Japan Geoscience Union Meeting 2018, Tokyo, Japan.

Seton, M., Flament, N., Whittaker, J., Müller, R. D., Gurnis, M., & Bower, D. J. (2015). Ridge subduction sparked reorganization of the Pacific plate-mantle system 60–50 million years ago. *Geophysical Research Letters, 42*(6), 1732-1740. doi:https://doi.org/10.1002/2015GL063057

Seton, M., Müller, R. D., Zahirovic, S., Gaina, C., Torsvik, T., Shephard, G., . . . Chandler, M. (2012). Global continental and ocean basin reconstructions since 200Ma. *Earth-Science Reviews, 113*(3), 212-270. doi:https://doi.org/10.1016/j.earscirev.2012.03.002

Shapiro, M. N., & Solov'ev, A. V. (2009). Formation of the Olyutorsky–Kamchatka foldbelt: a kinematic model. *Russian Geology and Geophysics, 50*(8), 668-681. doi:https://doi.org/10.1016/j.rgg.2008.10.006

Sigloch, K., & Mihalynuk, M. G. (2013). Intra-oceanic subduction shaped the assembly of Cordilleran North America. *Nature, 496*(7443), 50–56. doi:https://doi.org/10.1038/nature12019

Simmons, N. A., Myers, S. C., Johannesson, G., Matzel, E., & Grand, S. P. (2015). Evidence for long-lived subduction of an ancient tectonic plate beneath the southern Indian Ocean. *Geophysical Research Letters, 42*(21), 9270-9278. doi:https://doi.org/10.1002/2015GL066237

Simmons, N. A., Schuberth, B. S. A., Myers, S. C., & Knapp, D. R. (2019). Resolution and Covariance of the LLNL-G3D-JPS Global Seismic Tomography Model: Applications to Travel time Uncertainty and Tomographic Filtering of Geodynamic Models. *Geophysical Journal International, 217*(3), 1543-1557. doi:https://doi.org/10.1093/gji/ggz102

Steinberger, B., & Calderwood, A. R. (2006). Models of large-scale viscous flow in the Earth's mantle with constraints from mineral physics and surface observations. *Geophysical Journal International, 167*(3), 1461-1481. doi:https://doi.org/10.1111/j.1365-246X.2006.03131.x

Steinberger, B., & Holme, R. (2008). Mantle flow models with core-mantle boundary constraints and chemical heterogeneities in the lowermost mantle. *Journal of Geophysical Research: Solid Earth, 113*(B5), B05403. doi:https://doi.org/10.1029/2007JB005080

Steinberger, B., Torsvik, T. H., & Becker, T. W. (2012). Subduction to the lower mantle – a comparison between geodynamic and tomographic models. *Solid Earth, 3*(2), 415-432. doi:10.5194/se-3-415-2012

Stixrude, L., & Lithgow-Bertelloni, C. (2011). Thermodynamics of mantle minerals – II. Phase equilibria. *Geophysical Journal International, 184*(3), 1180-1213. doi:https://doi.org/10.1111/j.1365-246X.2010.04890.x

Thoraval, C., & Richards, M. A. (1997). The geoid constraint in global geodynamics: viscosity structure, mantle heterogeneity models and boundary conditions. *Geophysical Journal International, 131*(1), 1-8. doi:10.1111/j.1365-246X.1997.tb00591.x

Torsvik, T. H., Steinberger, B., Shephard, G. E., Doubrovine, P. V., Gaina, C., Domeier, M., . . . Sager, W. W. (2019). Pacific-Panthalassic Reconstructions: Overview, Errata and the Way Forward. *Geochemistry, Geophysics, Geosystems, 20*(7), 3659-3689. doi:10.1029/2019GC008402

Ueda, H., & Miyashita, S. (2005). Tectonic accretion of a subducted intraoceanic remnant arc in Cretaceous Hokkaido, Japan, and implications for evolution of the Pacific northwest. *The Island Arc, 14*, 582–598. doi:https://doi.org/10.1111/j.1440-1738.2005.00486.x

Vaes, B., van Hinsbergen, D. J. J., & Boschman, L. M. (2019). Reconstruction of Subduction and Back-Arc Spreading in the NW Pacific and Aleutian Basin: Clues to Causes of Cretaceous and Eocene Plate Reorganizations. *Tectonics, 38*(4), 1367-1413. doi:https://doi.org/10.1029/2018TC005164

van der Meer, D. G., Torsvik, T. H., Spakman, W., van Hinsbergen, D. J. J., & Amaru, M. L. (2012). Intra-Panthalassa Ocean subduction zones revealed by fossil arcs and mantle structure. *Nature Geoscience, 5*(3), 215-219. doi:https://doi.org/10.1038/ngeo1401

Van Der Meer, D. G., Zeebe, R. E., van Hinsbergen, D. J. J., Sluijs, A., Spakman, W., & Torsvik, T. H. (2014). Plate tectonic controls on atmospheric CO₂ levels since the Triassic. *Proceedings of the National Academy of Sciences, 111*(12), 4380. doi:10.1073/pnas.1315657111

Wang, H., Wang, Y., Gurnis, M., Zahirovic, S., & Leng, W. (2018). A long-lived Indian Ocean slab: Deep dip reversal induced by the African LLSVP. *Earth and Planetary Science Letters, 497*, 1-11. doi:https://doi.org/10.1016/j.epsl.2018.05.050

Whittaker, J. M., Müller, R. D., Leitchenkov, G., Stagg, H., Sdrolias, M., Gaina, C., & Goncharov, A. (2007). Major Australian-Antarctic Plate Reorganization at Hawaiian-Emperor Bend Time. *Science, 318*(5847), 83-86. doi:https://doi.org/10.1126/science.1143769

Wright, N. M., Seton, M., Williams, S. E., & Müller, R. D. (2016). The Late Cretaceous to recent tectonic history of the Pacific Ocean basin. *Earth-Science Reviews, 154*, 138-173. doi:https://doi.org/10.1016/j.earscirev.2015.11.015

Wu, F.-Y., Yang, J.-H., Xu, Y.-G., Wilde, S. A., & Walker, R. J. (2019). Destruction of the North China Craton in the Mesozoic. *Annual Review of Earth and Planetary Sciences, 47*(1), 173-195. doi:https://doi.org/10.1146/annurev-earth-053018-060342

Wu, J., Suppe, J., Lu, R., & Kanda, R. (2016). Philippine Sea and East Asian plate tectonics since 52 Ma constrained by new subducted slab reconstruction methods. *Journal of Geophysical Research: Solid Earth, 121*(6), 4670-4741. doi:https://doi.org/10.1002/2016JB012923

Wu, T.-J. J., & Wu, J. (2019). Izanagi-Pacific ridge subduction revealed by a 56 to 46 Ma magmatic gap along the northeast Asian margin. *Geology, 47*(10), 953-957. doi:https://doi.org/10.1130/G46778.1

Xinmin, Z., Tao, S., Weizhou, S., Liangshu, S., & Niu, Y. (2006). Petrogenesis of Mesozoic granitoids and volcanic rocks in South China: A response to tectonic evolution. *International Union of Geological Sciences, 29*(1), 26-33. doi:https://doi.org/10.18814/epiiugs/2006/v29i1/004

Yamasaki, T., & Nanayama, F. (2018). Immature intra-oceanic arc-type volcanism on the Izanagi Plate revealed by the geochemistry of the Daimaruyama greenstones in the Hiroo Complex, southern Hidaka Belt, central Hokkaido, Japan. *Lithos, 302-303*, 224-241. doi:https://doi.org/10.1016/j.lithos.2018.01.003

Zahirovic, S., Matthews, K. J., Flament, N., Müller, R. D., Hill, K. C., Seton, M., & Gurnis, M. (2016). Tectonic evolution and deep mantle structure of the eastern Tethys since the latest Jurassic. *Earth-Science Reviews, 162*, 293-337. doi:https://doi.org/10.1016/j.earscirev.2016.09.005

Zharov, A. E. (2005). South Sakhalin tectonics and geodynamics: A model for the Cretaceous-Paleogene accretion of the East Asian continental margin. *Russian Journal of Earth Sciences, 7*, ES5002.

Zhou, X. M., & Li, W. X. (2000). Origin of Late Mesozoic igneous rocks in Southeastern China: implications for lithosphere subduction and underplating of mafic magmas. *Tectonophysics, 326*(3), 269-287. doi:https://doi.org/10.1016/S0040-1951(00)00120-7